Double-electron excitation of H^- by fast proton and antiproton impact

Ken-ichi Hino*
Department of Applied Physics and Chemistry, The University of Electro-Communications, Chofu, Tokyo 182, Japan and Atomic Physics Laboratory, Institute of Physical and Chemical Research (RIKEN), Wako, Saitama 351-01, Japan

Mamoru Nagase,† Hiroyuki Okamoto, Toru Morishita, and Michio Matsuzawa
Department of Applied Physics and Chemistry, The University of Electro-Communications, Chofu, Tokyo 182, Japan

Mineo Kimura
Argonne National Laboratory, Argonne, Illinois 60439 and Department of Physics, Rice University, Houston, Texas 77251
(Received 8 November 1993)

A theoretical investigation is carried out for double-electron excitation processes of H^- induced by proton and antiproton impact at the energy of 1.5 MeV. Excitation cross sections to the $2s^2\,{}^1S^e$, $2s2p\,{}^1P^o$, and $2p^2\,{}^1D^e$ states are calculated by using the plane-wave Born approximation, the distorted-wave Born approximation, and the close-coupling method. Wave functions of H^- are generated employing the hyperspherical coordinate method. It is shown that the low-lying continuum $1skp\,{}^1P^o$ is identified as an important intermediate state in the double-electron excitation process to the $2p^2\,{}^1D^e$ state. We have also evaluated the ejected-electron spectra from the $2s2p\,{}^1P^o$ shape-resonance state. It is found that its spectral shape is close to the observed line profile of the photodetachment of H^- since the excitation mechanism to this state is mostly dominated by the optically allowed transition at the projectile energy concerned here.

PACS number(s): 34.50.Fa, 31.50.+w, 31.20.Tz

I. INTRODUCTION

Recent advance of experimental technique has made it possible to reveal evidences of the electron-electron correlation effect in the course of ion-atom collisions. Andersen *et al.* [1] made the first measurement of double ionization cross sections of He by antiproton ($\bar{p}$) impact in the energy range 0.5–5 MeV. They found that the cross section by the $\bar{p}$ impact dominates over that by the p impact by a factor of nearly 2, while the associated single ionization cross sections are almost the same. The conventional independent particle model cannot explain this observation because the leading term of the scattering amplitude by the Born series results in null contribution. Therefore, the striking difference of the cross sections suggests the importance of electron-electron correlation on the simultaneous two-electron ionization process.

This pioneering experiment highlights decisive roles of electron-electron correlation in the entire course of high energy ion-atom collisions [2]. A few years ago, Pedersen and Hvelplund [3] and Giese *et al.* [4] measured a set of double-electron excitation cross sections of He by e^-, p, and C^{q+} (q=4–6) impact from the ground state to the lowest-lying doubly excited states at the energies of 1.84 MeV/u and 1.5 MeV/u, respectively. Theoretical investigations on the excitation process have been done by Fritsch and Lin [5], Winter [6], Moribayashi *et al.* [7], and Slim *et al.* [8] by solving the coupled state equation of collision systems while Bachau *et al.* [9] and Straton *et al.* [10] studied the double-electron excitation processes of He in perturbative approaches. Their results also indicate the important role of the electron-electron correlation effect.

In accordance with the results by Moribayashi *et al.* [7], excitations to the lowest-lying doubly excited states of He by proton and antiproton impact at 1.5 MeV incident energy are mainly dominated by the first- and second-order mechanism through the optically allowed transition. Specifically, the $2s2p\,{}^1P^o$ state plays a decisive role as an intermediate state propagating into a set of final states $2s^2\,{}^1S^e$, $2p^2\,{}^1S^e$, and $2p^2\,{}^1D^e$. The simultaneous excitation of two electrons to this intermediate state by the first-order interaction with a projectile is understood to be due to the strong correlation effects. However, there appears only a small difference between cross sections of the p and $\bar{p}$ impacts in contrast to the double ionization mentioned above.

In the present article, we investigate double-electron excitation processes:

$$p\ (\bar{p}) + H^-(1s^2\,{}^1S^e)$$
$$\rightarrow p\ (\bar{p}) + H^{-**}(2s^2\,{}^1S^e,\ 2s2p\,{}^1P^o,\ 2p^2\,{}^1D^e)$$

at the projectile energy of 1.5 MeV. Our investigation on this collision system is motivated by the following three

*Present address: Department of Physics and Astronomy, University of Tennessee, 200 South College, Knoxville, TN 37996-1501.

†Present address: Berg Electronics Japan, Minami-Ohi, 3-28-10 Shinagawa-ku, Tokyo 140, Japan.

reasons. (1) The first is to understand the contributions of the electron-electron correlation of H^- to the collision dynamics and to examine if the same excitation mechanism as in the case of He holds during the collisions because the correlation effect of H^- is stronger than that of He. (2) The second is a comparison of the line profiles of ejected electron spectra decaying from the double-excited state $2s2p\ ^1P^o$ between the charged-particle and photon impacts. The $2s2p\ ^1P^o$ state in H^- is known to lie above the threshold energy of the manifold N=2 and it is the shape resonance [11–14]. This situation is different from that of He where the doubly excited $2s2p\ ^1P^o$ state is a Feshbach resonance. We investigate whether or not the line profile of the ejected electron is similar to that of photodetachment [15,16] at the present energy of a projectile ion since the dipole transition mainly dominates the excitation to the $2s2p\ ^1P^o$ state at high energy as is expected. (3) The third is to study the effect of the continuum such as the low-lying singly ionized state $1skp\ ^1P^o$ on double-electron excitation cross sections. It has been already suggested that this state has a great deal of contributions as an intermediate state to double-electron excitation processes of He [6]. Furthermore, the energy level scheme of H^- is simpler than that of He because of no singly excited states in H^-. Hence the p ($\bar{p}$)–H^- collision system is the best suited in which one can study the effect of the continuum.

In order to analyze details of collision dynamics and roles of correlations, the collision process is described by the close-coupling (CC) method, the first- and the second-order plane-wave Born approximations (PWBA1 and PWBA2), and the first- and the second-order distorted-wave Born approximations (DWBA1 and DWBA2) on the basis of the semiclassical impact-parameter picture. Wave functions of H^- are generated by the hyperspherical coordinate method based on the adiabatic approximation where the hyperradius of H^- is treated as an adiabatic parameter [17,18]. This method enables us to describe the electron correlation quite accurately [19,20]. In the study of double-electron excitation of He, Slim *et al.* [8] incorporated the continuum state and employed pseudostates to represent both the bound and the continuum contributions in their close-coupling calculation while we employ the hyperspherical wave functions for the bound and continuum states.

In the present calculations, we have made the two assumptions. First, doubly excited states of $2s^2\ ^1S^e$ and $2p^2\ ^1D^e$, though they are embedded in the continuum, are treated as discrete states. These are Feshbach resonances and have usually widths narrower than shape resonances do. This assumption is justified because of much shorter collision time (about 5 a.u. at the 1 MeV/u-impact) in comparison with decay lifetimes (of the order of 10^3 a.u.) of the associated autoionizing states [11–13, 21]. The second assumption is to neglect contributions from charge-transfer channels in describing a wave function of the whole collision system. This assumption is also valid because the direct excitation is dominant at the projectile energy studied here. For example, the charge-transfer cross section of p–H($1s$) system amounts to 1.29×10^{-22} cm^2 at the energy of 1.0 MeV using the continuum distorted wave approximation [22]. That of p–H^-($1s^2\ ^1S^e$) system is considered much smaller in the high energy region concerned here because of the smaller optimized Slater exponent of its $1s$ orbital. On the other hand, double-electron excitation cross sections of H^- are of the order of 10^{-20}–10^{-19}cm^2 as shown below.

The methods of calculations are given in Sec. II, where the method of discretizing continuum states is also described. Results and discussion are given in Sec. III, and concluding remarks are summarized in Sec. IV. Atomic units are used throughout unless otherwise stated.

II. METHODS OF CALCULATIONS

A. Atomic states employed

The wave function describing the whole collision system is expanded in terms of the H^- wave functions generated by the hyperspherical coordinate method. The wave functions of $^1S^e$,$^1P^o$, and $^1D^e$ states are generated by expanding the associated channel wave functions in terms of 25, 35, and 47 basis functions, respectively. Table I lists resulting energies of $1s^2\ ^1S^e$, $2s^2\ ^1S^e$, $2s2p\ ^1P^o$, and $2p^2\ ^1D^e$ states of H^- in comparison with other elaborate theoretical data [12,21,23–26]. Our present results agree with other calculations within the order of 0.1%.

Figure 1 shows behaviors of the adiabatic wave functions $F(R)$ of the $2s2p\ ^1P^o$ state at several energies against the hyperradius R. Oscillations of the wave functions begin at R equal to 40–90 a.u. Therefore, the electron densities are found to be localized within this inner R region. The continuum wave function of the $2s2p\ ^1P^o$ state is discretized into 10 and 20 meshes for the energy interval up to 0.0025 a.u. from threshold with $N = 2$ and included as basis functions in the expansion of the total wave function.

TABLE I. Energies (in Ry) of H^-. The entries in parentheses represent the width (in Ry) of the $2s2p\ ^1P^o$ state.

State	Present work	Other work
$1s^2\ ^1S^e$	-1.0527	-1.0555 [23]
$2s^2\ ^1S^e$	-0.2976	-0.2976 [25]
$2s2p\ ^1P^o$	-0.2488 (1.32×10^{-3})	-0.2487 (1.10×10^{-3}) [12]
		-0.2485 (1.37×10^{-3}) [24]
$2p^2\ ^1D^e$	-0.2550	-0.2559 [21]
		-0.2562 [26]

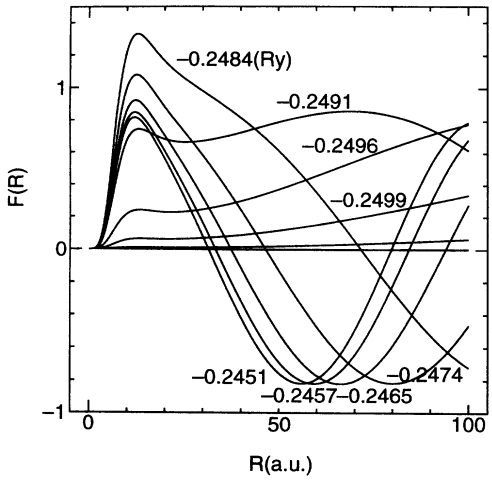

FIG. 1. The plots of the $2s2p\ ^1P^o$ shape resonance wave function $F(R)$ as the hyperradius R at the energies near the resonance energy. These are normalized to a unit amplitude at an asymptotic distance.

The low-lying singly ionized state $1skp\ ^1P^o$ just above the threshold with $N = 1$ is also incorporated into our basis set in order to study the effect on the double-electron excitation mechanism. The $1skp\ ^1P^o$ continuum is discretized into both 10 and 20 energy meshes up to 0.25 a.u. from the threshold energy -1 Ry of $N = 1$ to test the convergence of cross sections in the close-coupling calculation. It is assumed that the coupling of the $2s2p\ ^1P^o$ doubly excited states with the $1skp\ ^1P^o$ continuum near the resonance energy can be neglected. This assumption is reasonable for these continuum states because they do not overlap with the doubly excited states converging to the manifolds of $N = 2$.

The total wave function of the collision system is expanded in terms of 7, 37, 67, and 97 states of H^- for the test of convergence. A set of 7 states consists of all of the discrete states $1s^2\ ^1S^e, 2s^2\ ^1S^e$, and $2p^2\ ^1D^e$. A set of 37 states includes the $2s2p\ ^1P^o$ shape resonance which is discretized into 10 energy meshes in addition to the set of 7 states. Furthermore, the 67 state calculation includes the $1skp\ ^1P^o$ continuum discretized into 10 energy meshes in addition to the 37 state calculation. In order to test the effect of change of the mesh size, we have also made 97 state CC calculations for the following two sets: (i) 20 energy meshes for the $2s2p\ ^1P^o$ state and 10 energy meshes for the $1skp\ ^1P^o$ continuum and (ii) 10 energy meshes for the former and 20 energy meshes for the latter. Table II lists the sets of the atomic states employed for the close-coupling calculations, the PWBA2, and the DWBA2 approaches.

B. Collision dynamics

There is the residual long-range Coulomb interaction between a projectile ion and a target H^- even at large internuclear distance. Such a Coulomb scattering problem is properly dealt with by partitioning the asymptotic Coulomb tail $V_{\rm as}$ as a distortion potential from the projectile-target interaction V_P so that the perturbative interaction $\tilde{V}_P = V_P - V_{\rm as}$ is of short range [22, 27–29]. The asymptotic potential $V_{\rm as}$ is defined here as

$$V_{\rm as} = \frac{Z_P(Z_T - 2)}{X}, \tag{1}$$

with Z_P and Z_T being the nuclear charges of a projectile and H^-, respectively, and X being the internuclear distance of a collision system. The total wave function $\Psi^{(+)}(t)$ describing the collision system is expanded by

$$\Psi^{(+)}(t) = \sum_\alpha C_\alpha^{(+)}(t)\tilde{\psi}_\alpha^{(+)}(t). \tag{2}$$

It is understood that the summation over α includes the continuum states of H^-. Here the wave function $\tilde{\psi}_\alpha^{(+)}$ reads

$$\tilde{\psi}_\alpha^{(+)} = \psi_\alpha \exp(-i\sigma_+ - iE_\alpha t), \tag{3}$$

where σ_+ is the asymptotic Coulomb phase associated with $V_{\rm as}$ and satisfying the outgoing boundary conditions and ψ_α is a wave function of H^- with an eigenenergy of E_α. Substitution of Eq. (2) into the Schrödinger equation of the whole system yields the CC equation

$$i\frac{dC_\beta^{(+)}(t)}{dt} = \sum_\alpha C_\alpha^{(+)}(t)V_{\beta\alpha}\exp[i(E_\beta - E_\alpha)t], \tag{4}$$

where $V_{\beta\alpha} = \langle\psi_\beta|\tilde{V}_P|\psi_\alpha\rangle$. The initial condition

$$C_\rho^{(+)}(-\infty) = \delta_{\rho i} \tag{5}$$

TABLE II. Sets of atomic states included in the expansion of the total wave function for the description of the collision system.

Set	Atomic states included
7 states	$1s^2\ ^1S^e$, $2s^2\ ^1S^e$, $2p^2\ ^1D^e$ (5)
37 states	7 states plus $2s2p\ ^1P^o$ (3×10 meshes)
67 states	7 states plus $2s2p\ ^1P^o$ (3×10 meshes), $1skp\ ^1P^o$ (3×10 meshes)
97 states I	7 states plus $2s2p\ ^1P^o$ (3×20 meshes), $1skp\ ^1P^o$ (3×10 meshes)
97 states II	7 states plus $2s2p\ ^1P^o$ (3×10 meshes), $1skp\ ^1P^o$ (3×20 meshes)

is imposed on Eq. (4), where the subscript i means the ground state of H^-.

Substituting the scattering amplitude $C_\rho^{(+)}(t)$ with

$$\tilde{C}_\rho^{(+)}(t) = C_\rho^{(+)}(t)\exp\left(i\int_{-\infty}^{t} V_{\rho\rho}d\tau\right), \tag{6}$$

Eq. (4) is recast into the equivalent form

$$i\frac{d\tilde{C}_\beta^{(+)}(t)}{dt} = \sum_{\alpha\ (\neq\beta)} \tilde{C}_\alpha^{(+)}(t)V_{\beta\alpha} \times\exp\left[i(E_\beta - E_\alpha)t + i\int_{-\infty}^{t}(V_{\beta\beta} - V_{\alpha\alpha})d\tau\right]. \tag{7}$$

Expanding the scattering amplitude $C_\rho^{(+)}(t)$ of Eq. (4) up to the first and second order with respect to the perturbative potential $\tilde{V}_P$ leads to the PWBA1 and the PWBA2 approximations, respectively. Similarly, the DWBA1 and the DWBA2 approximations are obtained by expanding the scattering amplitude $\tilde{C}_\rho^{(+)}(t)$ of Eq. (7) up to the first and the second order with respect to the perturbative potential $\tilde{V}_P$, respectively.

The asymptotic Coulomb tail $V_{\rm as}$ in $\tilde{V}_P$ has significant effects on excitation cross sections calculated by the PWBA2. On the other hand, it should be noted that for the direct excitation cross sections obtained by the DWBA1, DWBA2, and CC, this potential is canceled out exactly in the phase factor of the right-hand side of Eq. (7).

C. Discretization of continuum states

We consider how to discretize continuum states into a scheme of finite energy meshes in our practical calculations. The total wave function of the collision system is expanded as shown in Eq. (2) by the complete set of target wave functions including both a bound state $\tilde{\psi}_B^{(+)}(t)$ and an energy-normalized continuum state $\tilde{\psi}_E^{(+)}(t)$, that is,

$$\Psi^{(+)}(t) = \sum_B C_B^{(+)}(t)\tilde{\psi}_B^{(+)}(t) + \int C_E^{(+)}(t)\tilde{\psi}_E^{(+)}(t)dE. \tag{8}$$

For the present purpose, we express the integral of the second term of Eq. (8) by a sum of integrals by introducing a sufficient small energy interval ΔE_n as follows:

$$\int C_E^{(+)}(t)\tilde{\psi}_E^{(+)}(t)dE = \sum_n \int_{E_n-\frac{\Delta E_n}{2}}^{E_n+\frac{\Delta E_n}{2}} C_E^{(+)}(t)\tilde{\psi}_E^{(+)}(t)dE \simeq \sum_n C_{E_n}^{(+)}(t)\sqrt{\Delta E_n}\tilde{\psi}_n^{(+)}(t), \tag{9}$$

where we have defined a wave packet $\tilde{\psi}_n^{(+)}$ as

$$\tilde{\psi}_n^{(+)}(t) = \frac{1}{\sqrt{\Delta E_n}}\int_{E_n-\frac{\Delta E_n}{2}}^{E_n+\frac{\Delta E_n}{2}} \tilde{\psi}_E^{(+)}(t)dE. \tag{10}$$

It should be noted that expression (10) for $\tilde{\psi}_n^{(+)}$ exactly satisfies the orthonormal relation

$$\langle\tilde{\psi}_n^{(+)}|\tilde{\psi}_{n'}^{(+)}\rangle = \delta_{n,n'}. \tag{11}$$

The discretized basis functions $\{\tilde{\psi}_n^{(+)}\}$ are spatially localized because of the uncertainty principle. In addition, this localized region should include the "reaction zone," within which the double-electron excitation processes are predominantly induced and the electron-electron correlation is substantial.

Here we refer to the matrix element $V_{EE'}$ of Eq. (4) between singly ionized states of ψ_E and $\psi_{E'}$. There is the case that the continuum-continuum matrix element $V_{EE'}$ is divergent when $E \simeq E'$. Nevertheless, the scattering amplitudes $C_E^{(+)}$ is always kept finite as shown in Appendix A. The contribution from a singly ionized state ψ_E to the scattering amplitude $C_E^{(+)}$ is given by Eqs. (A8) and (A10) at the asymptotic electron distance. This contribution may be negligible in our case since a velocity of a projectile we are concerned is much greater than a electron velocity of a continuum state and Eq. (A10) is zero. Thus a singly ionized state ψ_E contributes only from the inner region of the hyperradius R where the electron-electron correlation is dominant.

The arguments given above enable us to overcome the problems arising from the divergence of the continuum-continuum matrix element $V_{EE'}$, and hence we can evaluate it using the spatially localized wave function $\tilde{\psi}_n^{(+)}$ of Eq. (10). According to the discussion given in Appendix B, the wave packet is centered around $R = k_n|t|$ with k_n being the electron momentum associated with its energy E_n. If $|R \pm k_n t| < \frac{2k_n}{\Delta E_n}$, this can be approximately expressed by the representative component $\tilde{\psi}_{E_n}^{(+)}$ within the interval as

$$\tilde{\psi}_n^{(+)}(t) \simeq \sqrt{\Delta E_n}\tilde{\psi}_{E_n}^{(+)}(t). \tag{12}$$

If $|R \pm k_n t| \gg \frac{2k_n}{\Delta E_n}$, however, the wave function $\tilde{\psi}_n^{(+)}$ declines rapidly and has negligible effects. Thus we will adopt the expression of Eq. (12) hereafter in place of the exact expression of Eq. (10).

The discretization scheme given so far provides us with a well founded theoretical ground. As discussed in Appendix B, the wave packet of Eq. (12) is spatially localized mostly up to the maximum hyperradius $R_{\rm max}$, the choice of which should be compatible with the orthonormal condition of Eq. (11). For the $2s2p\ ^1P^o$ shape resonance, $R_{\rm max}$ given by Eq. (B5) amounts to about 10^3 a.u. if one takes an average mesh size $\Delta E_n \simeq 1.25\times10^{-4}$ a.u. as adopted in the 97 state I calculation. However, inspection of the continuum wave functions of H^- around the $2s2p\ ^1P^o$ resonance energy in Fig. 1 may enable one to relax the condition Eq. (B5) and to set $R_{\rm max} \simeq 100$ a.u. where the continuum wave functions show asymptotic behaviors.

In our actual calculation, we have carried out numerical integration using the Gauss-Legendre quadrature

with its weight coefficients in place of ΔE_n. Furthermore, we have introduced the damping factor λ into the wave function of Eq. (12) as $\tilde{\psi}_n^{(+)}\exp(-\lambda R)$ in order to accelerate the calculation of matrix elements and test whether or not the adopted $R_{\max}$ contains the reaction zone for the two-electron excitation processes. In order to confirm the insensitivity of our CC results with respect to change of $R_{\max}$ (equivalently, with respect to change of λ), we have made pilot calculations for $\lambda = 0$, 1/100, and 1/60 after fixing $R_{\max}$ at 100 a.u. They are found to agree with one another within a few percent, except for the $2p^2\ ^1D^e$ excitation where the relative difference is within some 15%. In later discussion, we employ the cross sections calculated with $R_{\max} = 100$ and $\lambda = 0$.

III. RESULTS AND DISCUSSION

To test the convergence of the double-electron excitation cross section with the number of the states included, we have made the calculations for the set of 7 states, 37 states, 67 states, and two sets of 97 states given in Table II. Comparison of the 67 state results with those by two sets of the 97 states I and II shows that they agree with one another within a few percent. One of our main concerns is the line shape of the $2s2p\ ^1P^o$ ejected electron spectra. Hence, hereafter, we employ the results calculated using the 97 states I because a finer mesh scheme has been adopted for the discretization of the $2s2p\ ^1P^o$ shape resonance.

A. Total cross sections to $2s^2\ ^1S^e$ and $2p^2\ ^1D^e$ states

Table III gives the calculated excitation cross sections to the $2s^2\ ^1S^e$ and $2p^2\ ^1D^e$ states at the energy of 1.5 MeV by using the PWBA1, PWBA2, DWBA1, DWBA2, and CC.

TABLE III. Double-electron excitation cross section (in units of 10^{-20} cm^2) of H^- to the $2s^2\ ^1S^e$ and the $2p^2\ ^1D^e$ states at the energy of 1.5 MeV.

Method	Proton	Antiproton
	$2s^2\ ^1S^e$	
PWBA1	9.589	9.589
PWBA2 (97 states)	15.521	14.675
DWBA1	9.509	9.566
DWBA2 (97 states)	9.593	9.472
CC (7 states)	9.483	9.548
CC (37 states)	9.394	9.236
CC (67 states)	9.842	9.856
CC (97 states)	9.691	9.656
	$2p^2\ ^1D^e$	
PWBA1	0.466	0.466
PWBA2 (97 states)	1.446	1.393
DWBA1	0.423	0.465
DWBA2 (97 states)	1.286	1.580
CC (7 states)	0.483	0.481
CC (37 states)	0.488	0.568
CC (67 states)	1.307	1.299
CC (97 states)	1.234	1.429

First, we discuss the cross section to the $2s^2\ ^1S^e$ state. Apart from the result by the PWBA2, the cross sections obtained by the PWBA1, DWBA1, DWBA2, and CC are nearly equal to one another as seen from Table III. The deviation of the PWBA2 results from other approaches implies that the plane-wave Born expansion is not accurate enough while the PWBA1 results qualitatively reproduce the converged results by the CC. Indeed, we have found that the diagonal parts of the matrix elements of $\tilde{V}_P$ for $1s^2\ ^1S^e$ and $2s^2\ ^1S^e$ states have much greater magnitudes than the off-diagonal parts of the matrix elements of $\tilde{V}_P$. Hence, for the present case, we cannot justify the PWBA2 expansion which treats all the matrix elements on the equal footing, i.e., as small perturbations.

The DWBA1 and DWBA2 approximations can remedy these difficulties since the dominant diagonal matrix elements are incorporated to all orders and the remaining small off-diagonal ones are reasonably dealt with as small perturbations. In the present case, the distorted-wave Born expansion is valid and the results are compatible with the CC results.

The static potential $V_{\rho\rho}$ in Eq. (6) gives the energy shift from the eigenenergy E_ρ of the state ρ. The energy shift arises from the polarization effect induced by an electric field of a projectile. Such an effect of the static potential on H^- may be ascribable to the fact that its electron density extends up to the relatively distant region and the two electrons are weakly bound on a proton. Hence the present situation is much different from that of He where the collision dynamics is reasonably interpreted by the PWBA2 approach consistent with the CC calculation [7].

As a result, we obtain the cross section to the $2s^2\ ^1S^e$ state by the PWBA1 method close to those by the DWBA1, DWBA2, and CC methods even if the diagonal matrix elements themselves are relatively large. Then we consider that most effects from the non-negligible diagonal matrix elements are canceled out by the introduction of the phase factor in Eq. (6) resulting in quite small overall contributions to the cross sections obtained. According to this argument, the doubly excited state $2s^2\ ^1S^e$ is mainly produced by the first-order interaction with a projectile, namely, the monopole transition. Consequently, there is merely a small difference between the cross sections by the p and $\bar{p}$ impacts.

Next, we discuss the results for the $2p^2\ ^1D^e$ state excitation. Large difference between the results obtained by the PWBA2, DWBA2, and CC and those by the PWBA1 and DWBA1 shown in Table III clearly suggests that the $2p^2\ ^1D^e$ state is produced by the two-step mechanism through intermediate states of H^-. Let us shed light on the roles played by the intermediate $1skp\ ^1P^o$ and $2s2p\ ^1P^o$ continuum states to analyze the details of the collision dynamics. We consider the results of calculations by the CC method with a set of 7, 37, 67, and 97 states. (See Sec. II A for more details on the atomic states included in the expansion and see also Table II.)

The 37 state CC calculation that includes the $2s2p\ ^1P^o$ shape resonance gives the $2p^2\ ^1D^e$ excitation cross section almost equal to those for the 7 state CC calculation,

while the 67 state CC calculation yields the $2p^2\ ^1D^e$ excitation cross section two to three times larger than the 37 state CC calculation. A comparison of the results by the 67 state with the 97 state confirms that our calculated cross sections converge reasonably within a few percent. This means that at the incident energy of 1.5 MeV, the $1skp\ ^1P^o$ state has dominant contribution as an intermediate state to the double-electron excitation while the $2s2p\ ^1P^o$ state has little effect.

In the double-electron excitation of He to the $2p^2\ ^1D^e$ state, it was seen that the $2s2p\ ^1P^o$ state as well as the $1s2p\ ^1P^o$ singly excited state plays a key role as an intermediate state [7]. Here it is found that the low-energy continuum of the $1skp\ ^1P^o$ state plays the most important role as intermediate states, which is an equivalent role by the singly excited $1s2p\ ^1P^o$ state of He, while the $2s2p\ ^1P^o$ shape resonance does not. This is probably because the overlap matrix element between the $1s^2\ ^1S^e$ state and the low-energy $1skp\ ^1P^o$ state is fairly large.

B. Spectral line profile of an ejected electron from the $2s2p^1P^o$ state

We have calculated the spectral line profiles of an ejected electron from the $2s2p\ ^1P^o$ shape resonance state caused by the p and $\bar{p}$ impacts using the 97 state CC expansion. At the energy of 1.5 MeV, the line profiles are quite similar to those obtained by the PWBA1 and DWBA1, so that there is only a small difference between the cases of the p and $\bar{p}$ impacts. Hence the double-electron excitation to this state is induced by the first-order interaction with a projectile, namely, the optically allowed transition. Therefore we show only the spectral line profile of the $2s2p\ ^1P^o$ shape resonance state by the p impact in Fig. 2.

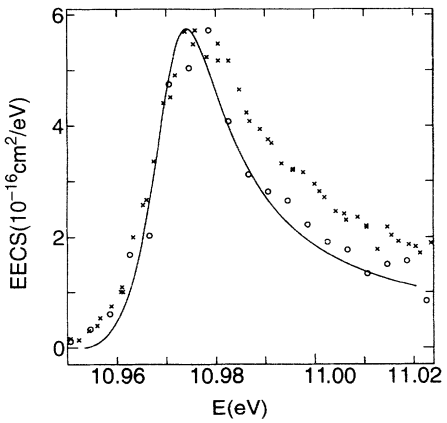

FIG. 2. Spectral line profile of the electron-emission cross section (EECS) from the $2s2p\ ^1P^o$ state by proton impact at the incident energy of 1.5 MeV. This figure also includes a comparison of the calculated spectra of an electron by proton impact with the experimental line profile by photodetachment: open circles, Halka *et al.* [30]; crosses, Butterfield [31]. The photodetachment data are normalized at the peak position of our results. The excitation energy E is gauged from the ground state of H^- and is calculated based on the ground state energy by Pekeris [23] and the Rydberg constant for the hydrogen atom $R_H = R_\infty/(1 + m_e/M_p) = 13.598\,27$ eV.

Figure 2 compares the shapes of the line profile caused by the p impact at 1.5 MeV with the line profile by the photodetachment of H^- for decay into the $H(N = 2)$ channel observed by Halka *et al.* [30] and Butterfield [31], where the experimental data are normalized at the peak position of our theoretical results. Photodetachment spectra of H^- in this energy region are in good agreement with theoretical studies [15,24,32]. The calculated profile is in good agreement with the improved data by Halka *et al.* [30]. This good agreement confirms the dominance of the dipole allowed transition to the double-electron excitation to the $2s2p^1P^o$ state at high energy.

IV. CONCLUDING REMARKS

We have calculated the excitation cross sections to the doubly excited states of H^- at the incident energy of 1.5 MeV using the plane-wave Born expansion, the distorted-wave Born expansion, and the close-coupling method. The wave functions of H^- for expanding the total wave function of the collision system are generated by the hyperspherical coordinate method. The continuum wave functions are included in basis sets with energy discretization. Excitation to the $2s^2\ ^1S^e$ state proceeds by the first-order interaction with a projectile through the monopole transition. However, it should be noted that the plane-wave Born expansion is not justified here since the diagonal parts of the potential matrix elements are much larger than the off-diagonal parts. Hence the diagonal and off-diagonal matrix elements should not be dealt with on the equal footing. Excitation to the $2p^2\ ^1D^e$ state is understood as the two-step mechanism via the dipole transition. Particularly, the $1skp\ ^1P^o$ states are important as an intermediate state. We have evaluated spectral line profiles of an ejected electron decaying from the $2s2p\ ^1P^o$ shape resonance state. The first-order interaction via the dipole transition is found to predominate over the collision dynamics in the excitation process to this state. The spectral shapes of the line profile obtained by the p and $\bar{p}$ impacts are in reasonable agreement with the observation of the associated photodetachment spectra.

ACKNOWLEDGMENTS

We would like to express our appreciation to the Institute of Physical and Chemical Research (RIKEN) for use of computer facilities for numerical calculations. We also gratefully acknowledge the helpful discussion with S. Watanabe and the assistance in the final stage of numerical calculations by J. Sato. This research has been supported by the international cooperative research program between the National Science Foundation and the Japan Society for the Promotion of Science. This work is partly supported by Grant-in-Aid for Scientific Research on Priority Areas "Theory of Chemical Reaction-Computational Approach" from the Ministry of Education, Science and Culture of Japan. The work is also supported in part by the U. S. Department of Energy, Office of Health and Environmental Research under Contract No. W31-109-Eng-38.

APPENDIX A

In this appendix, we assess the contribution of the potential matrix element $V_{EE'}$ bracketed by singly ionized states ψ_E and $\psi_{E'}$ to the scattering amplitude in Eq. (4). The continuum-continuum matrix element is not always finite, that is, there is the case that this gives a divergent contribution since the electron density of a continuum electron extends over the whole positional space unless the appropriate wave packet is adopted. We show below that the scattering amplitude is always defined finite even if the matrix element is divergent. Although this problem was analyzed three decades ago by Seaton [33] in the study of the electron-atom collision, we shall briefly describe an outline of the method mentioned in the text.

Here it is understood that the eigenenergies of the singly ionized states are expressed as $E = \epsilon - \frac{1}{2N^2}$ and $E' = \epsilon' - \frac{1}{2N'^2}$, respectively, at the asymptotic distance of two electrons, with ϵ and ϵ' being the energies of continuum electrons and N and N' being the manifolds of the residual hydrogen atom. We concern ourselves only with the asymptotic r region where the present divergent problem becomes serious. Let wave functions of continuum electrons be represented by $\phi_\epsilon(r)$ and $\phi_{\epsilon'}(r)$, respectively. These wave functions are energy normalized as defined by

$$\int \phi^*_\epsilon(r)\phi_{\epsilon'}(r)dr = \delta(\epsilon - \epsilon'). \tag{A1}$$

The continuum-continuum matrix element $V_{EE'}$ is considered to be not divergent as long as ϵ is much different from ϵ', the manifolds of the residual hydrogen atom are not the same, namely, $N \neq N'$, or the angular momentum for expanding the projectile-electron potential V_P by partial waves is not zero. Otherwise the matrix element will be divergent. Therefore, our consideration is limited to the monopole transition, i.e., to the case that the matrix element is expressed by

$$V_{\epsilon\epsilon'} = -\frac{2Z_P f_{\epsilon\epsilon'}(X)}{X}, \tag{A2}$$

where

$$f_{\epsilon\epsilon'}(X) = \int_X^\infty \left(\frac{X}{r} - 1\right)\phi^*_\epsilon(r)\phi_{\epsilon'}(r)dr \tag{A3}$$

and $\epsilon \simeq \epsilon'$. Here $V_{\epsilon\epsilon'}$ has been replaced for $V_{EE'}$ since we consider the case of $N = N'$.

The wave function $\phi_\epsilon(r)$ at the asymptotic distance is expressed as

$$\phi_\epsilon(r) \simeq \sqrt{\frac{2}{\pi k}}\sin[kr + \delta_l(\epsilon)], \tag{A4}$$

where k is the momentum of an electron with $\epsilon = \frac{k^2}{2}$. Here the phase shift $\delta_l(\epsilon)$ is expressed by $\delta_l(\epsilon) \simeq \delta_l(0) + \epsilon\tau_l(\epsilon)$ with $\tau_l(\epsilon)$ being the time duration defined by $\tau_l(\epsilon) = \frac{d\delta_l(\epsilon)}{d\epsilon}$. Inserting Eq. (A4) into the expression Eq. (A3), we obtain

$$f_{\epsilon\epsilon'}(X) = \frac{1}{\pi\sqrt{kk'}}\int_X^\infty \left(\frac{X}{r} - 1\right) \times \{\cos[(k-k')(r+k\tau_l)] - \cos[(k+k')r + 2\delta_l(\epsilon)]\}dr. \tag{A5}$$

Contributions from $\cos[(k+k')r + 2\delta_l(\epsilon)]$ may be neglected because the rapid oscillation cancels out the integrand. Performing the integration by parts with respect to r leads Eq. (A5) to

$$f_{\epsilon\epsilon'}(X) = \frac{X}{\sqrt{kk'}}\int_X^\infty \frac{1}{r^2}\frac{\sin[(k-k')(r+k\tau_l)]}{\pi(k-k')}dr - \delta(\epsilon - \epsilon'). \tag{A6}$$

Equation (A6) shows that the matrix element $V_{\epsilon\epsilon'}$ is divergent.

We pay attention to the term including the divergent matrix element in the right-hand side of the CC equation, Eq. (4), that is,

$$F_\epsilon(t) = \int d\epsilon' C^{(+)}_{\epsilon'}(t)V_{\epsilon\epsilon'}\exp[i(\epsilon - \epsilon')t]. \tag{A7}$$

Employing Eqs. (A2) and (A6), Eq. (A7) is cast into the form

$$F_\epsilon(t) \simeq \frac{-2Z_P C^{(+)}_\epsilon(t)}{X}\zeta_\epsilon(t), \tag{A8}$$

where

$$\zeta_\epsilon(t) = \int_X^\infty dr\frac{X}{r^2}\int_0^\infty d\epsilon'\frac{1}{\sqrt{kk'}}\frac{\sin[(k-k')(r+k\tau_l)]}{\pi(k-k')} \times\exp[i(\epsilon - \epsilon')t] - 1. \tag{A9}$$

The ϵ' integration of Eq. (A9) is easily carried out to get $\theta(r - k(|t| - \tau_l))$. Consequently, we have obtained

$$\zeta_\epsilon(t) = \left(\frac{X}{k(|t| - \tau_l)} - 1\right)\theta(k(|t| - \tau_l) - X) \tag{A10}$$

and shown that $F_\epsilon(t)$, related to the continuum-continuum interaction, is always kept finite. According to Eq. (A10), $\zeta_\epsilon(t)$ has a physical meaning associated with the screening effect due to an projectile ion against a continuum electron if the electron momentum is larger than the velocity of the projectile in the case of $\tau_l \simeq 0$. If $\tau_l \gg 1$, the expression Eq. (A10) may be related with the effect of the postcollision interaction [34, 35].

APPENDIX B

Herein we will make further discussion on the wave packet of Eq. (10) and derive the expressions of Eq. (12). At the asymptotic distance, the continuum wave function $\tilde{\psi}^{(+)}_E$ reads

$$\tilde{\psi}^{(+)}_E \simeq \sqrt{\frac{2}{\pi k}}\sin(kR + \delta), \tag{B1}$$

where a bound-state wave function of a residual hydrogenic atom and the residual Coulomb phase σ_+ are omitted for simplicity and $E = \frac{k^2}{2}$. Inserting Eq. (B1) into Eq. (10), we obtain

$$\tilde{\psi}_n^{(+)} \simeq \frac{\sqrt{\Delta E_n}}{2i}\sqrt{\frac{2}{\pi k_n}}\left(e^{i(k_nR+\delta_n)}\frac{\sin\xi_-}{\xi_-} - e^{-i(k_nR+\delta_n)}\frac{\sin\xi_+}{\xi_+}\right)e^{-iE_nt}. \tag{B2}$$

Here $\xi_\pm = \frac{\Delta E_n}{2k_n}\rho_\pm$ and $\rho_\pm = R \pm k_n t$. In the region where the condition $\xi_\pm \gg 1$, namely, $\rho_\pm \gg \frac{2k_n}{\Delta E_n}$ is satisfied, the wave packet $\tilde{\psi}_n^{(+)}$ declines rapidly and then this effect is negligible here. Therefore, the wave packet has an effective contribution only in the localized region where $\xi_\pm < 1$. We may approximate $\tilde{\psi}_n^{(+)}$ in this region as the representative component $\tilde{\psi}_{E_n}^{(+)}$, that is,

$$\tilde{\psi}_n^{(+)} \simeq \sqrt{\Delta E_n}\tilde{\psi}_{E_n}^{(+)}, \tag{B3}$$

where use has been made of the approximation $\frac{\sin\xi_\pm}{\xi_\pm} \simeq 1$. This expression is identical to Eq. (12).

We can consider that the wave packet is spatially localized at most up to the maximum hyperradius $R_{\max}$ owing to the discussion given above. $R_{\max}$ may be determined so that the approximated wave packet of Eq. (B3) retrieves the orthonormal condition of Eq. (11). Using Eqs.(B1) and (B3), we obtain

$$\langle\tilde{\psi}_n^{(+)}|\tilde{\psi}_{n'}^{(+)}\rangle \simeq \frac{1}{\pi}\sqrt{\frac{\Delta E_n \Delta E_{n'}}{k_n k_n'}} \times\left(\frac{\sin(K_-R_{\max}+\Delta_-)-\sin\Delta_-}{K_-} - \frac{\sin(K_+R_{\max}+\Delta_+)-\sin\Delta_+}{K_+}\right). \tag{B4}$$

Here $K_\pm$ and $\Delta_\pm$ are defined as $k_n \pm k_{n'}$ and $\delta_n \pm \delta_{n'}$, respectively. In general, the second term in the parentheses of Eq. (B4) may be neglected under the condition $K_+ \gg 1$. Thus we will consider only the first term hereafter. The left-hand side of Eq. (B4) must be unity when $n = n'$, namely, $K_- = \Delta_- = 0$. This leads to the relation

$$R_{\max} \simeq \frac{\pi k_n}{\Delta E_n}. \tag{B5}$$

Next we consider the case that $N \equiv n - n' \neq 0$. Using approximations $\frac{\Delta E_n}{k_n} \approx \frac{\Delta E_{n'}}{k_{n'}}$ and $K_- \approx N\frac{\Delta E_n}{k_n}$ with Eq. (B5), Eq. (B4) becomes of the form

$$\langle\tilde{\psi}_n^{(+)}|\tilde{\psi}_{n'}^{(+)}\rangle \simeq \frac{\sin\Delta_-}{\pi N}. \tag{B6}$$

This shows that the approximated wave function of Eq. (B3) almost satisfies the orthogonal condition when taking reasonably fine mesh points for the energy discretization, specifically, at the vicinity of a resonance.

[1] L. H. Andersen, P. Hvelplund, H. Knudsen, S. P. Møller, K. Elsener, K.-G.Rensfelt, and E. Uggerhøj, Phys. Rev. Lett. **57**, 2147 (1986).
[2] J. H. McGuire, Adv. At. Mol. Phys. **29**, 217 (1992).
[3] J. O. P. Pedersen and P. Hvelplund, Phys. Rev. Lett. **62**, 2373 (1989).
[4] J. P. Giese, M. Schulz, J. K. Swenson, H. Schöne, M. Benhenni, S. L. Varghese, C. R. Vane, P. F. Ditter, S. M. Shafroth, and S. Datz, Phys. Rev. A **42**, 1231 (1990).
[5] W. Fritsch and C. D. Lin, Phys. Rev. A **41**, 4776 (1990).
[6] T. G. Winter, Phys. Rev. A **43**, 4727 (1991).
[7] K. Moribayashi, K. Hino, M. Matsuzawa, and M. Kimura, Phys. Rev. A **44**, 7234 (1991); **45**, 7922 (1992); **46**, 1684 (1992); **47**, 4874 (1993).
[8] H. A. Slim, B. H. Bransden, and D. R. Flower, J. Phys. B **26**, L159 (1993).
[9] H. Bachau, M. Bahri, F. Martin, and A. Salin, J. Phys. B **24**, 2015 (1991).
[10] J. C. Straton, J. H. McGuire, and Z. Chen, Phys. Rev. A **46**, 5514 (1992).
[11] A. J. Taylor and P. G. Burke, Proc. Phys. Soc. **92**, 336 (1967).
[12] P. G. Burke, A. J. Taylor, and S. Ormonde, Proc. Phys. Soc. **92**, 345 (1967).
[13] J. H. Macek and P. G. Burke, Proc. Phys. Soc. **92**, 351 (1967).
[14] C.D. Lin, Phys. Rev. Lett. **35**, 1150 (1975).
[15] J. T. Broad and W. P. Reinhardt, Phys. Rev. A **14**, 2159 (1976).
[16] J. H. Macek, Proc. Phys. Soc. **92**, 365 (1967).
[17] J. H. Macek, J. Phys. B **1**, 831 (1968).
[18] C. D. Lin, Adv. At. Mol. Phys. **22**, 77 (1986).
[19] N. Koyama, H. Fukuda, T. Motoyama, and M. Matsuzawa, J. Phys. B **19**, L331 (1986).
[20] H. Fukuda, N. Koyama, and M. Matsuzawa, J. Phys. B **20**, 2959 (1987).
[21] P. G. Burke, Adv. At. Mol. Phys. **4**, 173 (1968).
[22] Dž. Belkić, R. Gayat, and A. Salin, Phys. Rep. **56**, 279 (1979).
[23] C. L. Pekeris, Phys. Rev. **126**, 1470 (1962).
[24] H. R. Sadeghpour, C. H. Greene, and M. Cavagnero, Phys. Rev. A **45**, 1587 (1992).
[25] A. K. Bhatia and A. Temkin, Phys. Rev. **153**, 177 (1967).
[26] A. K. Bhatia and A. Temkin, Phys. Rev. A **11**, 2018 (1975).
[27] D. P. Dewangan and J. Eichler, J. Phys. B **18**, L65 (1985); **19** 2939 (1986).
[28] Dž. Belkić, S. Saini, and H. Taylor, Phys. Rev. A **36**, 1601 (1987).
[29] D. P. Dewangan and B. Bransden, J. Phys. B **21**, L353 (1988).
[30] M. Halka, H. C. Bryant, Carol Johnstone, B. Marchini, W. Miller, A. H. Mohagheghi, C. Y. Tang, K. B. Butterfielde, D. A. Clark, S. Cohen, J. B. Donahue, P. A. M. Gram, R. W. Hamm, A. Hsu, D. W. MacArthur, E. P. MacKerrow, C. R. Quick, J. Tiee and K. Rózsa, Phys. Rev. A **46**, 6942 (1992).
[31] K. B. Butterfield, cited in M. Halka *et al.* (Ref. [30]).
[32] J. Z. Tang, H. Wakabayashi, M. Matsuzawa, S. Watanabe, and I. Shimamura, Phys. Rev. A **49**, 1021 (1994).
[33] M. J. Seaton,*Atomic and Molecular Processes* edited by D. R. Bates, (Academic, New York, 1962), pp. 374–420, particularly see its appendix.
[34] R. Morgenstern, A. Niehaus, and U. Thielmann, J. Phys. B **10**, 1039 (1977).
[35] A. Niehaus, J. Phys. B **10**, 1845 (1977).